Journal of Sound and Vibration (1991) **146**(1), 135–156

INTERACTIONS BETWEEN TIME-VARYING MESH STIFFNESS AND CLEARANCE NON-LINEARITIES IN A GEARED SYSTEM

A. KAHRAMAN† AND R. SINGH

Department of Mechanical Engineering, The Ohio State University, 206 West 18th Avenue, Columbus, Ohio 43210-1107, U.S.A.

(*Received 3 January 1990, and in revised form 20 June 1990*)

Frequency response characteristics of a non-linear geared rotor–bearing system with time-varying mesh stiffness $k_h(\bar{t})$ are examined in this paper. First, the single-degree-of-freedom spur gear pair model with backlash is extended to include sinusoidal or periodic mesh stiffness $k_h(\bar{t})$. Second, a three-degree-of-freedom model with $k_h(\bar{t})$ and clearance non-linearities associated with gear backlash and rolling element bearings, as excited by the static transmission error $\bar{e}(\bar{t})$ under a mean torque load, is developed. The governing equations are solved using digital simulation technique and only the primary resonances are studied. Resonances of the corresponding linear time-varying system associated with parametric and external excitations are identified using the method of multiple scales and digital simulation. Interactions between the mesh stiffness variation and clearance non-linearities have been investigated; a strong interaction between time-varying mesh stiffness $k_h(\bar{t})$ and gear backlash is found, whereas the coupling between $k_h(\bar{t})$ and bearing non-linearities is weak. Finally, our time-varying non-linear formulations yield reasonably good predictions when compared with the benchmark experimental results available in the literature.

1. INTRODUCTION

Dynamic models of geared systems can be classified into four main groups. The first group includes linear time-invariant (LTI) models, as evident from an extensive review of the literature given in reference [1]. In the second group linear time-varying (LTV) mesh stiffness $k_h(\bar{t})$ is included in the analysis [2–9]. The periodic variation in $k_h(\bar{t})$ is due to the change of the number of conjugate teeth pairs in contact during the convolute action. Accordingly, the system is excited parametrically as well as by the static transmission error $\bar{e}(\bar{t})$ introduced by kinematic errors and tooth deflections. In this case, the equation of motion of the gear pair essentially reduces to Mathieu's or Hill's equation with a periodic external forcing function. The third group includes gear backlash in the models, but with time-invariant average mesh stiffness $k_h \neq k_h(\bar{t})$ [10–18]. It should be noted that backlash is bound to exist either by design or due to manufacturing errors and/or wear in any gear pair. Finally, in the last group both gear backlash and mesh stiffness variation are considered simultaneously [19–25]. However, none of these studies have addressed explicitly the effect of $k_h(\bar{t})$, including its interaction with the backlash non-linearity, on the steady state frequency response. Ozguven and Houser [19] have attempted to analyze this problem by replacing $k_h(\bar{t})$ with a constant mesh stiffness and by defining the "loaded static transmission error" excitation at the mesh point. But

† Currently with the General Motors Research Laboratories, Power Systems Research Department, 30500 Mound Road, Warren, Michigan 48090-9055, U.S.A.

0022-460X/91/070135+22 $03.00/0

Ozguven [26] has stated recently that this approach may not work depending on the system parameters, and recommended a detailed investigation of this issue.

Numerous publications have analyzed LTV systems [27–29] and time-varying systems with quadratic and/or cubic non-linearities [30–33]. However, such studies are not directly applicable to the geared rotor systems which are the main focus of this paper; this problem requires the solution to a set of time-varying differential equations with clearance-type non-linearities as excited by a periodic force generated at the gear mesh.

2. PROBLEM FORMULATION

A generic geared rotor–bearing system, which consists of a spur gear pair mounted on flexible shafts, supported by rolling element bearings as shown in Figure 1(a), is considered here. The gearbox is assumed to be rigid. The effect of the prime mover or the load inertia is not considered, assuming that such inertial elements are connected to the gearbox through soft torsional couplings. Furthermore, we assume that the system is symmetric about the plane of the gears and that the axial motion (parallel to the shafts) is negligible. The governing equations of motion can be given in matrix form as

$$[\bar{M}]\{\bar{q}''(\bar{t})\}+[\bar{C}]\{\bar{q}'(\bar{t})\}+[\bar{K}(\bar{t})]\{f(\bar{q}(\bar{t}))\}=\{\bar{F}(\bar{t})\}, \tag{1}$$

where $[\bar{M}]$ is the time-invariant mass matrix and $\{\bar{q}(\bar{t})\}$ is the displacement vector. Here,

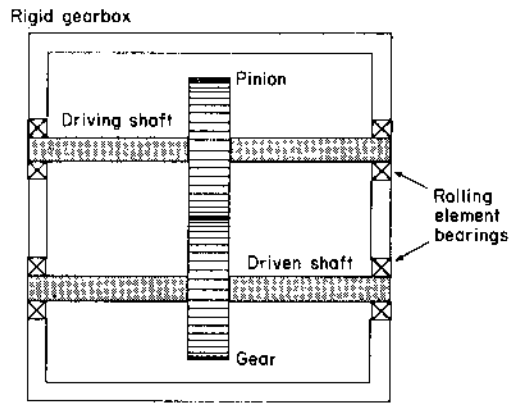

(a)

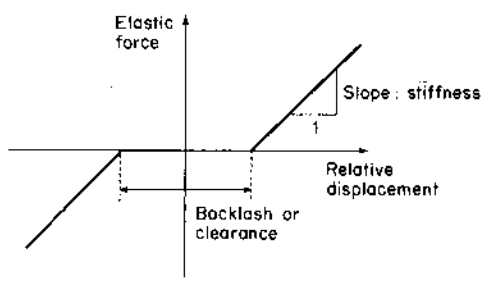

(b)

Figure 1. (a) Generic geared rotor-bearing system; (b) clearance non-linearity in gears and bearings.

damping matrix $[\bar{C}]$ is assumed to be time-invariant, as the effect of the tooth separation and time-varying mesh properties on mesh damping are considered to be negligible; the validity of this assumption will be examined later. The stiffness matrix $[\bar{K}(\bar{t})]$ is considered to be a periodically time-varying matrix given by $[\bar{K}(\bar{t})]=[\bar{K}(\bar{t}+2\pi/\bar{\Omega}_h)]$, where $\bar{\Omega}_h$ is the fundamental gear mesh frequency. The non-linear displacement vector $\{f(\bar{q}(\bar{t}))\}$ includes the radial clearances in bearings and the gear backlash as shown in Figure 1(b), and the forcing vector $\{\bar{F}(\bar{t})\}$ consists of both external torque and internal static transmission error excitations. (A list of symbols is given in the Appendix.)

This paper extends our previous non-linear single-degree-of-freedom spur gear pair [10] and multi-degree-of-freedom geared rotor-bearing system [11] models by including time-varying mesh stiffness $k_h(\bar{t})$, and investigates its effect on the frequency response of lightly and heavily loaded geared systems. Interactions between mesh stiffness variation and system non-linearities associated with gear backlash and radial clearances in rolling element bearings are also considered. The resonances of the corresponding LTV system associated with the parametric and external excitations are identified using the method of multiple scales. Our formulation will be validated by comparing predictions with available experimental results [2, 34].

3. MATHEMATICAL MODEL

A reduced order form of the multi-degree-of-freedom system of equation (1), the three-degree-of-freedom non-linear model of the geared rotor system, which has been

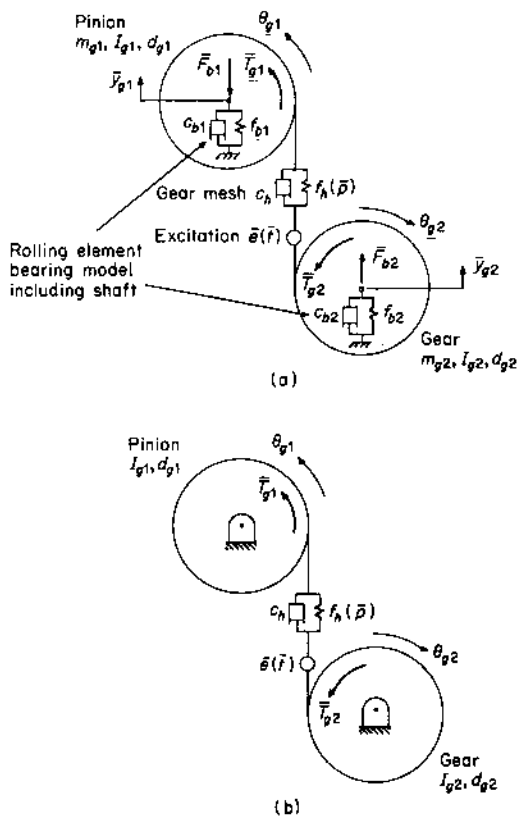

Figure 2. Non-linear models of the geared system of Figure 1: (a) three-degree-of-freedom system; (b) gear pair model with a single degree of freedom.

used in our previous study [11], is considered here. This includes gear inertias I_{g1} and I_{g2}, gear masses m_{g1} and m_{g2}, and base circle diameters d_{g1} and d_{g2}, as shown in Figure 2(a). The gear mesh is described by a non-linear displacement function f_h with time-varying stiffness $k_h(\bar{t})$ and linear viscous damping c_h. The bearings and the shafts that support the gears are modeled by equivalent elements with viscous damping coefficients c_{b1} and c_{b2} and non-linear springs defined by force-displacement functions f_{b1} and f_{b2} which are approximated by piecewise linear, dead zone type non-linearities as suggested in reference [11]. Both low-frequency external excitation due to torque fluctuations and high-frequency internal excitation due to the static transmission error $\bar{e}(\bar{t})$ are considered in the formulation [11]. The input torque fluctuation is included, but the output torque is assumed to be constant: i.e. $\bar{T}_{g1}(\bar{t}) = \bar{T}_{g1m} + \bar{T}_{g1a}(\bar{t})$ and $\bar{T}_{g2}(\bar{t}) = \bar{T}_{g2m}$. External radial preloads $\bar{F}_{b1}$ and $\bar{F}_{b2}$ are also applied to both rolling element bearings.

3.1. EQUATIONS OF MOTION

The equations of coupled transverse-torsional motion of the geared rotor-bearing system shown in Figure 2(a) with the displacement vector $\{\bar{q}(\bar{t})\} = \{\bar{y}_{g1}(\bar{t}), \bar{y}_{g2}(\bar{t}), \bar{p}(\bar{t})\}$ are given in matrix form as follows [11]:

$$\begin{bmatrix} m_{g1} & 0 & 0 \\ 0 & m_{g2} & 0 \\ -m_{c1} & m_{c1} & m_{c1} \end{bmatrix} \begin{Bmatrix} \bar{y}''_{g1}(\bar{t}) \\ \bar{y}''_{g2}(\bar{t}) \\ \bar{p}''(\bar{t}) \end{Bmatrix} + \begin{bmatrix} c_{b1} & 0 & c_h \\ 0 & c_{b2} & -c_h \\ 0 & 0 & c_h \end{bmatrix} \begin{Bmatrix} \bar{y}'_{g1}(\bar{t}) \\ \bar{y}'_{g2}(\bar{t}) \\ \bar{p}'(\bar{t}) \end{Bmatrix}$$
$$+ \begin{bmatrix} k_{b1} & 0 & k_h(\bar{t}) \\ 0 & k_{b2} & -k_h(\bar{t}) \\ 0 & 0 & k_h(\bar{t}) \end{bmatrix} \begin{Bmatrix} f_{b1}(\bar{y}_{g1}(\bar{t})) \\ f_{b2}(\bar{y}_{g2}(\bar{t})) \\ f_h(\bar{p}(\bar{t})) \end{Bmatrix} = \begin{Bmatrix} -\bar{F}_{b1} \\ \bar{F}_{b2} \\ \bar{F}_m - m_{c1}\bar{e}''(\bar{t}) + \bar{F}_{aT}(\bar{t}) \end{Bmatrix}, \tag{2a}$$

$$\bar{p}(\bar{t}) = (d_{g1}/2)\theta_{g1}(\bar{t}) - (d_{g2}/2)\theta_{g2}(\bar{t}) + \bar{y}_{g1}(\bar{t}) - \bar{y}_{g2}(\bar{t}) - \bar{e}(\bar{t}), \tag{2b}$$

$$m_{c1} = 1 \Big/ \left(\frac{d_{g1}^2}{4I_{g1}} + \frac{d_{g2}^2}{4I_{g2}} \right), \qquad \bar{F}_m = \frac{2\bar{T}_{g1m}}{d_{g1}} = \frac{2\bar{T}_{g2m}}{d_{g2}}, \qquad \bar{F}_{aT}(\bar{t}) = \frac{m_{c1}\bar{T}_{g1a}(\bar{t})}{2I_{g1}}, \tag{2c-e}$$

$$k_h(\bar{t}) = k_h(\bar{t} + 2\pi/\bar{\Omega}_h) = k_{hm} + \sum_{r=1}^{\infty} k_{har} \cos(r\bar{\Omega}_h\bar{t} + \phi_{hr}), \tag{2f}$$

$$f_{bi}(\bar{y}_{gi}) = \begin{cases} \bar{y}_{gi} - b_{bi}, & \bar{y}_{gi} > b_{bi} \\ 0, & -b_{bi} < \bar{y}_{gi} < b_{bi} \\ \bar{y}_{gi} + b_{bi}, & \bar{y}_{gi} < -b_{bi} \end{cases}, \qquad f_h(\bar{p}) = \begin{cases} (\bar{p} - b_h), & \bar{p} > b_h \\ 0, & -b_h < \bar{p} < b_h \\ (\bar{p} + b_h), & \bar{p} < -b_h \end{cases}. \tag{2g, h}$$

Here $(\,)'$ denotes a derivative with respect to time $\bar{t}$, $\bar{y}_{gi}$ and $\bar{\theta}_{gi}$ are the transverse and torsional displacements of the ith gear ($i = 1, 2$), m_{c1} is the equivalent gear pair mass, $\bar{F}_m$ is the average force transmitted through the gear mesh, and $\bar{F}_{aT}(t)$ is the fluctuating force related to the external input torque excitation. Equations (2a–h) have been used previously by us in reference [11] except for the $k_h(\bar{t})$ term, which is expanded in equations (2a–h) in the Fourier series form. Here $\bar{p}(\bar{t})$ is the difference between the dynamic transmission error and the static transmission error $\bar{e}(\bar{t})$. A dimensionless form of equation (2a) is obtained by letting $y_{gi}(\bar{t}) = \bar{y}_{gi}(\bar{t})/b_c$, $p(\bar{t}) = \bar{p}(\bar{t})/b_c$, $\omega_n = \sqrt{k_{hm}/m_{c1}}$, $\omega_{bi} = \sqrt{k_{bi}/m_{gi}}$ ($i = 1, 2$) and $t = \omega_n\bar{t}$, where b_c is the characteristic length. Here, we consider periodic excitation for both $\bar{e}(\bar{t})$ and $\bar{F}_{aT}(\bar{t})$ as $\bar{e}(\bar{t}) = \sum_{r=1}^{\infty} \bar{e}_r \cos(r\bar{\Omega}_h\bar{t} + \phi_{er})$, $\bar{F}_{aT}(\bar{t}) = \sum_{r=1}^{\infty} \bar{F}_{aTr} \cos(r\bar{\Omega}_T\bar{t} + \phi_{Tr})$, where $\bar{\Omega}_h$ and $\bar{\Omega}_T$ are the fundamental excitation frequencies of internal displacement and external torque fluctuations, respectively. Furthermore, dimensionless excitation frequencies $\Omega_h = \bar{\Omega}_h/\omega_n$ and $\Omega_T = \bar{\Omega}_T/\omega_n$ are defined. The

governing equations of motion can then be written in the dimensionless form

$$\begin{bmatrix} 1 & 0 & 0 \\ 0 & 1 & 0 \\ -1 & 1 & 1 \end{bmatrix} \begin{Bmatrix} \ddot{y}_{g1}(t) \\ \ddot{y}_{g2}(t) \\ \ddot{p}(t) \end{Bmatrix} + 2 \begin{bmatrix} \zeta_{11} & 0 & \zeta_{13} \\ 0 & \zeta_{22} & -\zeta_{23} \\ 0 & 0 & \zeta_{33} \end{bmatrix} \begin{Bmatrix} \dot{y}_{g1}(t) \\ \dot{y}_{g2}(t) \\ \dot{p}(t) \end{Bmatrix} + \begin{bmatrix} \kappa_{11} & 0 & \kappa_{13}(t) \\ 0 & \kappa_{22} & -\kappa_{23}(t) \\ 0 & 0 & \kappa_{33}(t) \end{bmatrix} \begin{Bmatrix} f_{b1}(y_{g1}) \\ f_{b2}(y_{g2}) \\ f_h(p) \end{Bmatrix}$$

$$= \begin{Bmatrix} -F_{b1} \\ F_{b2} \\ F_m \end{Bmatrix} + \begin{Bmatrix} 0 \\ 0 \\ F_{ah}(t) \end{Bmatrix} + \begin{Bmatrix} 0 \\ 0 \\ F_{aT}(t) \end{Bmatrix}, \tag{3a}$$

$$F_{ah}(t) = \sum_{r=1}^{\infty} F_{ahr}(r\Omega_h)^2 \cos(r\Omega_h t + \phi_{er}), \qquad F_{ahr} = \frac{\tilde{e}_r}{b_c}, \tag{3b, c}$$

$$F_{aT}(t) = \sum_{r=1}^{\infty} F_{aTr} \cos(r\Omega_T t + \phi_{Tr}), \qquad F_{aTr} = \frac{\tilde{F}_{aTr}}{m_{c1} b_c \omega_n^2}, \tag{3d, e}$$

$$F_m = \bar{F}_m / m_{c1} b_c \omega_n^2, \quad F_{bi} = \bar{F}_{bi} / m_{gi} b_c \omega_n^2, \qquad i = 1, 2, \tag{3f, g}$$

$$\zeta_{ii} = c_{bi} / 2 m_{gi} \omega_n, \qquad \zeta_{i3} = c_h / 2 m_{gi} \omega_n, \quad i = 1, 2, \qquad \zeta_{33} = c_h / 2 m_{c1} \omega_n, \tag{3h-j}$$

$$\kappa_{ii} = \frac{\omega_{bi}^2}{\omega_n^2}, \qquad \kappa_{i3}(t) = \frac{k_h(t)}{m_{gi} \omega_n^2}, \quad i = 1, 2, \tag{3k, l}$$

$$\kappa_{33}(t) = \frac{k_h(t)}{k_{hm}} = 1 + \sum_{r=1}^{\infty} \varepsilon_r \cos(r\Omega_h t + \phi_{hr}), \tag{3m}$$

$$f_{bi}(y_{gi}) = \begin{cases} y_{gi} - b_{bi}/b_c, & y_{gi} > b_{bi}/b_c \\ 0, & -b_{bi}/b_c < y_{gi} < b_{bi}/b_c \\ y_{gi} + b_{bi}/b_c & y_{gi} < -b_{bi}/b_c \end{cases}, \tag{3n}$$

$$f_h(p) = \begin{cases} p - b_h/b_c, & p > b_h/b_c \\ 0, & -b_h/b_c < p < b_h/b_c \\ p + b_h/b_c, & p < b_h/b_c \end{cases}. \tag{3o}$$

Here F_{bi} $(i = 1, 2)$ and F_m are the dimensionless components of the mean force vector $\{F\}_m$, and $F_{aT}(t)$ and $F_{ah}(t)$ pertain to the alternating external excitation $\{F(t)\}_e$ and the internal excitation $\{F(t)\}_i$ force vectors, respectively.

4. GEAR PAIR STUDIES

First, we consider the spur gear pair model of reference [10], as shown in Figure 2(b), and investigate the effect of $k_h(\bar{t})$ on the steady state frequency response. The equation of motion of the gear pair is obtained from equation (3a) by substituting $y_{gi}(t) = 0$ for fixed gear centers. Neglecting the input torque variations for the sake of convenience, $F_{aT}(t) = 0$, we obtain the following equation of motion of a loaded gear pair with time-varying mesh stiffness and backlash, as excited by the static transmission error:

$$\ddot{p}(t) + 2\zeta_{33}\dot{p}(t) + \kappa_{33}(t) f_h(p(t)) = F_m + F_{ah}(t). \tag{4}$$

Here ζ_{33}, $\kappa_{33}(t)$, $f_h(p)$, F_m and F_{ah} are still given by equation (3). Since none of the existing analytical solution methods are found to be suitable for this problem, a digital simulation technique has been used to solve equation (4). A fifth-sixth order Runge-Kutta numerical integration algorithm with variable time step [35] was used here. This technique

had previously been employed successfully for the gear pair problem with time-invariant mesh stiffness [10].

First consider only sinusoidally varying mesh stiffness and the static transmission error excitation: i.e., $\kappa_{33}(t) = 1 + \varepsilon \cos(\Omega_h t + \phi_{h1})$, where $\varepsilon = \varepsilon_1$ and $F_{ah}(t) = F_{ah1}\Omega_h^2 \cos(\Omega_h t + \phi_{e1})$. The tooth deflection or $F_{ah}(t)$ is maximum under the applied mean load F_m when $\kappa_{33}(t)$ is minimum (i.e., minimum number of gear pairs in contact). Similarly, minimum $F_{ah}(t)$ corresponds to maximum $\kappa_{33}(t)$. Therefore, there is an out-of-phase relationship between $F_{ah}(t)$ and $\kappa_{33}(t)$: i.e., $\phi_{h1} = \phi_{e1} + \pi$. Here, we set $\phi_{h1} = \pi$ and $\phi_{e1} = 0$ for the sake of convenience. Hence, equation (4) is modified to

$$\ddot{p}(t) + 2\zeta_{33}\dot{p}(t) + [1 - \varepsilon \cos(\Omega_h t)] f_h(p(t)) = F_m + F_{ah}\Omega_h^2 \cos(\Omega_h t). \tag{5}$$

4.1. LINEAR TIME-VARYING (LTV) SYSTEM

For zero gear backlash b_h, the gear mesh displacement function is $f_h(p) = p$. Hence equation (5) reduces to an LTV equation as follows:

$$\ddot{p}(t) + 2\zeta_{33}\dot{p}(t) + [1 - \varepsilon \cos \Omega_h t)] p(t) = F_m + F_{ah}\Omega_h^2 \cos(\Omega_h t). \tag{6}$$

Approximate analytical solutions of similar LTV differential equations with parametric and external excitations have already been given in the literature [27, 28, 30–33]. Therefore we have not attempted to solve equation (6) completely. Instead we have identified the corresponding resonances by using the method of multiple scales [27]. The first order uniform solution is given by an expansion having the following form, where the scalar parameter ε is assumed to be very small;

$$p(t; \varepsilon) = p_0(T_0, T_1) + \varepsilon p_1(T_0, T_1) + O(\varepsilon^2). \tag{7}$$

Here $T_n = \varepsilon^n t$ is the nth time scale. The expansions for the derivatives with respect to t are obtained in terms of the partial derivatives with respect to time scales $D_n = \partial/\partial T_n$:

$$\mathrm{d}/\mathrm{d}t = D_0 + \varepsilon D_1 + O(\varepsilon^2), \qquad \mathrm{d}^2/\mathrm{d}t^2 = D_0^2 + 2\varepsilon D_0 D_1 + O(\varepsilon^2). \tag{8a, b}$$

Substituting equations (7) and (8) into equation (6) and equating like powers of ε, with the external force being applied at $O(\varepsilon^0)$, one obtains

$$D_0^2 p_0 + p_0 = F_m + F_{ah1}\Omega_h^2 \cos(\Omega_h T_0), \qquad D_0^2 p_1 + p_1 = -2D_0 D_1 p_0 - \mu D_0 p_0 + p_0 \cos(\Omega_h T_0), \tag{9a, b}$$

where $\varepsilon\mu = 2\zeta_{33}$. The solution of equation (9a) is given in the complex domain as

$$p_0 = A(T_1)\, \mathrm{e}^{\mathrm{i}T_0} + F_m + \Lambda\, \mathrm{e}^{\mathrm{i}\Omega_h T_0} + cc, \qquad \Lambda = F_{ah1}\Omega_h^2/2(1 - \Omega_h^2), \tag{10a, b}$$

where cc represents the complex conjugate terms and $\mathrm{i} = \sqrt{-1}$. At $\Omega_h \approx 1$, we note that $(1 - \Omega_h^2)^{-1}$ will make the amplitude of the response boundless; this is the primary resonance since it appears in the first order. Substituting equation (10) into equation (9b) we obtain

$$D_0^2 p_1 + p_1 = -2\mathrm{i}D_1 A\, \mathrm{e}^{\mathrm{i}T_0} - \mathrm{i}\mu A\, \mathrm{e}^{\mathrm{i}T_0} - \mathrm{i}\mu\Lambda\Omega_h\, \mathrm{e}^{\mathrm{i}\Omega_h T_0} + \tfrac{1}{2}A\, \mathrm{e}^{\mathrm{i}(1+\Omega_h)T_0} + \tfrac{1}{2}A\, \mathrm{e}^{\mathrm{i}(1-\Omega_h)T_0} + \tfrac{1}{2}\Lambda\, \mathrm{e}^{2\mathrm{i}\Omega_h T_0} + \tfrac{1}{2}F_m\, \mathrm{e}^{\mathrm{i}\Omega_h T_0} + \Lambda + cc. \tag{11}$$

Besides the primary resonance at $\Omega_h \approx 1$, the particular solution of equation (11) has other secular terms when $2\Omega_h \approx 1$ and $\Omega_h \approx 2$. At $2\Omega_h \approx 1$, summation of the external excitation frequency and the parametric excitation frequency is close to the dimensionless natural frequency which is unity. One should also observe resonances at $\Omega_h \approx n$, $n > 2$ when higher scales are considered in equation (7). In summary, equation (6) has resonances at $\Omega_h \approx 0{\cdot}5$ and n, where $n = 1, 2, 3, \ldots$.

Equation (6) has been solved by using digital simulation. In Figure 3 are shown the steady state frequency response curves $p_a(\Omega_h)$ and $p_m(\Omega_h)$ for a lightly loaded system with $F_m = 0{\cdot}1$, $F_{ah1} = 0{\cdot}05$, $\zeta_{33} = 0{\cdot}05$, $b_h = 0$ and four different ε values. Note that $\varepsilon = 0$ represents the LTI system. For $\varepsilon > 0$, we do not observe any multi-valued regions and jump phenomenon, similar to those seen for the non-linear systems. The mesh stiffness variation ε has a negligible effect on the natural frequency which corresponds to the largest peak in Figure 3(a), but an increase in ε amplifies p_a in both resonance and off-resonance regions. Here p_m is no longer uncoupled from p_a, and it varies substantially in the vicinity of primary resonance at $\Omega_h = 1{\cdot}0$, and the parametric resonance at $\Omega_h = 0{\cdot}5$, especially for a large ε, confirming the analysis given earlier. Note that our study is limited to only these two resonances, as an investigation of subharmonic resonances at $\Omega_h \approx n$, $n > 1$ is beyond the scope of this study.

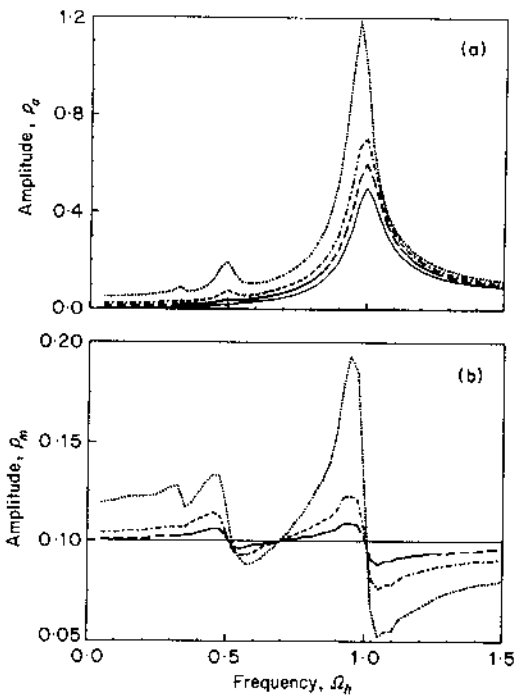

Figure 3. Frequency response spectra of a lightly loaded LTV gear pair with sinusoidal $\bar{e}(\bar{t})$ and $k_h(\bar{t})$; $F_m = 0{\cdot}1$, $F_{ah1} = 0{\cdot}05$, $\zeta_{33} = 0{\cdot}05$, $b_h = 0$ and four different ε values: (a) p_a versus Ω_h; (b) p_m versus Ω_h. ——, $\varepsilon = 0$; – – –, $\varepsilon = 0{\cdot}1$; — · —, $\varepsilon = 0{\cdot}2$; · · · ·, $\varepsilon = 0{\cdot}4$.

4.2. NON-LINEAR TIME-VARYING SYSTEM

Next we consider the time-varying non-linear system with backlash, given by equation (5). In Figure 4 are shown $p_a(\Omega_h)$ and $p_m(\Omega_h)$ spectra with $F_m = 0{\cdot}1$, $F_{ah1} = 0{\cdot}05$, $\zeta_{33} = 0{\cdot}05$ and four ε values. In this case, we notice a jump discontinuity at the resonant frequency and a dual-valued region bounded by jump-up and jump-down transition frequencies. For $\varepsilon = 0$, p_m is independent of Ω_h in the no-impact regime, similar to the results given in reference [10]. But when $\varepsilon > 0$, the transition frequencies which define the jump phenomenon become smaller, and p_a at the jump-down frequency grows with increasing ε. This indicates that $k_h(\bar{t})$ enhances the degree of non-linearity associated with the gear

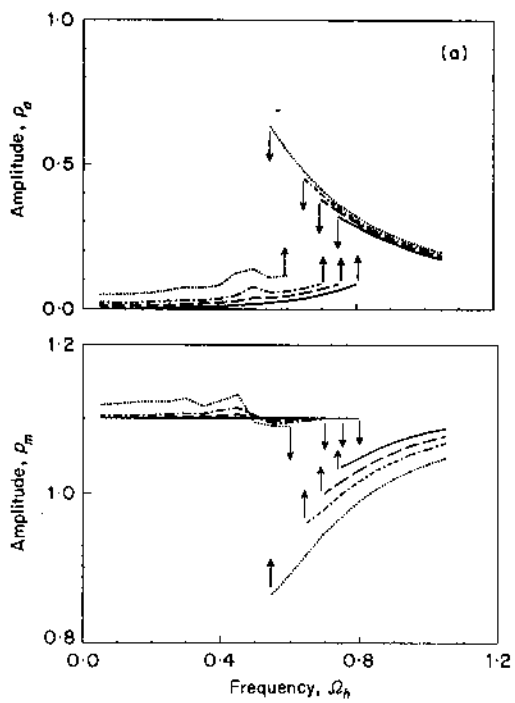

Figure 4. Frequency response spectra of the lightly loaded non-linear gear pair of Figure 2(b) with sinusoidal $\bar{e}(\bar{t})$ and $k_h(\bar{t})$; $F_m = 0{\cdot}1$, $F_{ah} = 0{\cdot}05$, $\zeta_{33} = 0{\cdot}05$, $b_h = b_c$ and four different ε values: (a) p_a versus Ω_h; (b) p_m versus Ω_h. Key as Figure 3.

backlash. Similar to the results of LTV system in Figure 3, we again observe in Figure 4(a) a parametric resonance at $\Omega_h = 0{\cdot}5$, which is strong for $\varepsilon = 0{\cdot}2$ and $0{\cdot}4$ curves. The time histories $p(t)$ for each ε value at the parametric resonance peak, $\Omega_h = 0{\cdot}5$, are compared in Figure 5. For the LTI system ($\varepsilon = 0$), a harmonic no-impact type steady state solution exists, as illustrated in Figure 5(a). With increasing ε, this solution is

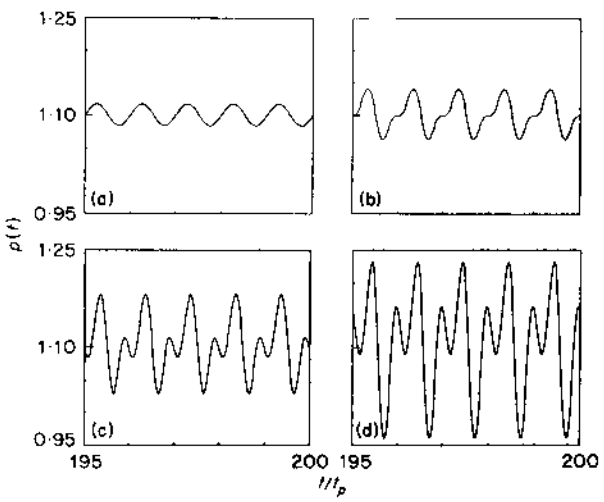

Figure 5. Steady state time histories corresponding to $\Omega_h = 0{\cdot}5$ in Figure 4: (a) $\varepsilon = 0$ (LTI model); (b) $\varepsilon = 0{\cdot}1$; (c) $\varepsilon = 0{\cdot}2$; (d) $\varepsilon = 0{\cdot}4$. Here, $t_p = 2\pi/\Omega_h$.

transformed into a non-harmonic periodic solution with a larger peak-to-peak value as a result of the parametric mesh stiffness excitation, as shown in Figures 5(b–d).

Now, consider a heavily loaded gear pair with $F_m = 0{\cdot}1$, $F_{ah1} = 0{\cdot}01$ and $\zeta_{33} = 0{\cdot}05$. $p_a(\Omega_h)$ and $p_m(\Omega_h)$ spectra are shown in Figures 6(a) and 6(b), respectively. In this case, tooth separation does not occur for $\varepsilon = 0$, which results in a linear frequency response curve with a constant p_m. A small jump is seen at $\varepsilon = 0{\cdot}1$, and this jump becomes larger for $\varepsilon = 0{\cdot}2$ and $0{\cdot}4$; overall alternating amplitudes p_a at resonance and within the off-resonance regions increase considerably. This suggests that the mesh stiffness variation is especially important for a heavily loaded gear pair with backlash.

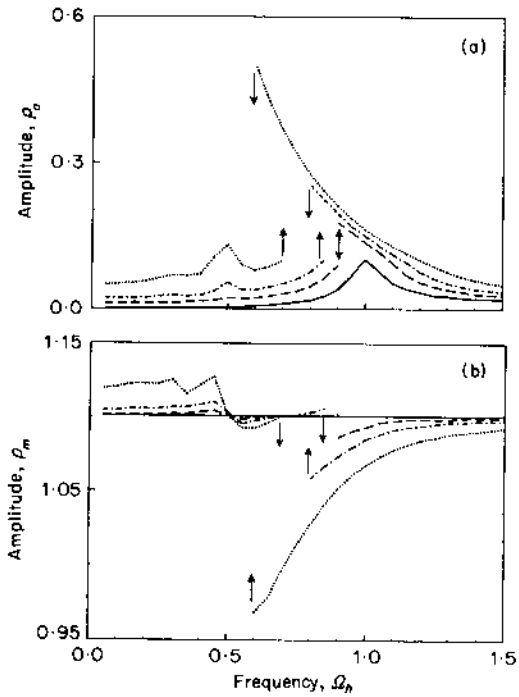

Figure 6. Frequency response spectra of a heavily loaded non-linear gear pair with sinusoidal $\bar{e}(\bar{t})$ and $k_h(\bar{t})$; $F_m = 0{\cdot}1$, $F_{ah1} = 0{\cdot}01$, $\zeta_{33} = 0{\cdot}05$, $b_h = b_c$ and four different ε values: (a) p_a versus Ω_h; (b) p_m versus Ω_h. Key as Figure 3.

4.3. NON-LINEAR TIME-VARYING MESH DAMPING

In order to investigate the effect of non-linear, time-varying gear mesh damping on the steady state frequency response, we consider a sinusoidally varying gear mesh damping $\zeta_{33}(t)$ which is assumed to be proportional to the mesh stiffness function $\kappa_{33}(t)$, and a non-linear velocity function g_h associated with tooth separation. Hence the governing equation of motion is

$$\ddot{p}(t) + 2\zeta_{33}(t) g_h(\dot{p}(t)) + [1 - \varepsilon \cos(\Omega_h t)] f_h(p(t)) = F_m + F_{ah}\Omega_h^2 \cos(\Omega_h t), \quad (12a)$$

$$\zeta_{33}(t) = \zeta_{33}\kappa_{33}(t) = \zeta_{33}(1 + \varepsilon \cos(\Omega_h t + \phi_{h1})), \quad (12b)$$

$$g_h(\dot{p}(t)) = \begin{cases} 0, & -b_h/b_c < p < b_h/b_c \\ \dot{p}(t), & \text{otherwise} \end{cases}. \quad (12c)$$

In Figure 7 frequency response spectra are compared for the cases of (a) non-linear time-varying gear mesh damping defined by equation (12), and (b) linear time-invariant

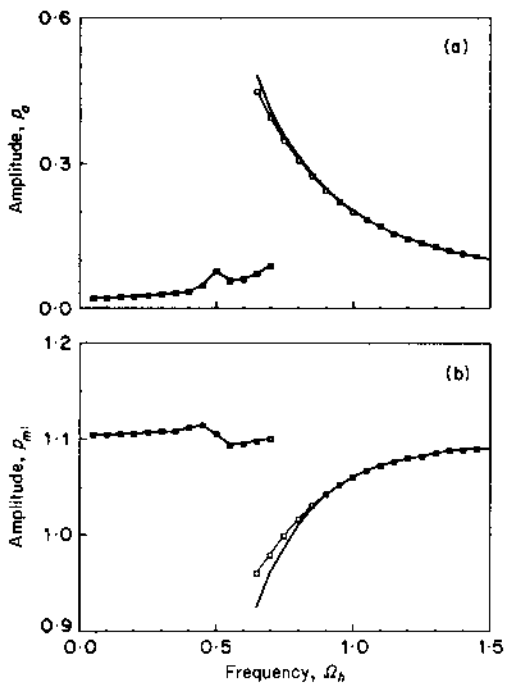

Figure 7. Frequency response spectra of gear pair corresponding to non-linear time-varying (——) and linear viscous (—□—) damping models: (a) p_a versus Ω_h; (b) p_m versus Ω_h.

mesh damping $\zeta_{33}$with $g_h(\dot{p}(t)) = \dot{p}(t)$, as given by equation (5). As shown in Figure 7, both mesh damping models yield virtually the same spectra. Therefore a linear time-invariant gear mesh damping model can be used without losing any accuracy.

4.4 PERIODIC $\bar{e}(\bar{t})$ AND $k_h(\bar{t})$

Up to now, we have considered only the sinusoidally varying $k_h(\bar{t})$ and $\bar{e}(\bar{t})$. In real geared systems, however, both $k_h(\bar{t})$ and $\bar{e}(\bar{t})$ are periodic and can be expressed in Fourier series form. $k_h(\bar{t})$ and $\bar{e}(\bar{t})$ for a low contact ratio spur gear pair are illustrated in Figure 8; these typical time histories were predicted by using an existing spur gear tooth model [36]. The first six Fourier coefficients of $k_h(\bar{t})$ and $\bar{e}(\bar{t})$ are given in Table 1. Note that the nth harmonic of $\bar{e}(\bar{t})$ causes a resonance around $\Omega_h = 1/n$. Hence higher harmonics are important only at low frequencies. Accordingly, only the first three Fourier coefficients of $\bar{e}(\bar{t})$ are deemed to be sufficient here, given the nature of the practical gear noise and vibration problems. Similarly, $k_h(\bar{t})$ is also truncated for the sake of convenience, with the first three terms retained. Higher terms ($n > 3$) could be easily included in the analysis if necessary. Therefore the governing equation with $F_{aT}(t) = 0$ is

$$\ddot{p}(t) + 2\zeta_{33}(t)\dot{p}(t) + \left[1 - \sum_{r=1}^{3} \varepsilon_r \cos(r\Omega_h t)\right] f_h(p(t)) = F_m + \sum_{r=1}^{3} F_{ahr}(r\Omega_h)^2 \cos(r\Omega_h t). \tag{13}$$

In Figures 9(a) and 9(b) are shown frequency response spectra for $F_m = 0{\cdot}1$, $F_{ah1} = 0{\cdot}05$, $F_{ah2} = 0{\cdot}02$, $F_{ah3} = 0{\cdot}01$, $\zeta_{33} = 0{\cdot}05$, $\varepsilon_1/\varepsilon_2 = 2$, $\varepsilon_1/\varepsilon_3 = 4$ and four different $\varepsilon_1 = \varepsilon$ values. As shown in Figure 9, two other jump discontinuities, which are clearly associated with F_{ah2} and F_{ah3}, are found. These jumps are similar to the fundamental resonance peak except that they have lower amplitudes. In order for these two jumps to exist, F_{ah2} and F_{ah3}

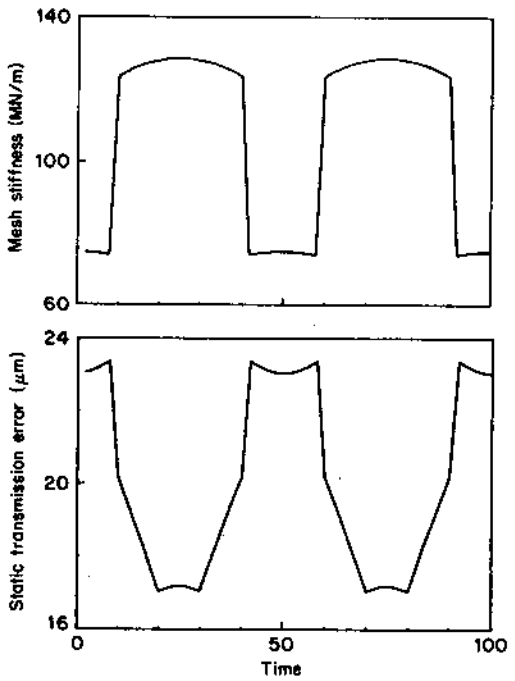

Figure 8. $\bar{e}(\bar{t})$ and $k_h(\bar{t})$ plots for a low contact ratio spur gear pair [36]. Here the number of teeth is 28, the diametral pitch is eight, the pressure angle is 20 degrees, and a 6×10^{-4} in tip modification starting at 26 degrees roll angle is applied.

excitations have to be large. Once again, it is evident that the periodic mesh stiffness enhances the extent of backlash non-linearity.

5. GEARED ROTOR-BEARING SYSTEM STUDIES

Next, we solved the three-degree-of-freedom non-linear model of Figure 2(a) and equation (3a) by using the digital simulation technique for excitation $F_{ah}(t)$ with $F_{aT}(t)=0$.

TABLE 1

Fourier coefficients of $\bar{e}(\bar{t})$ and $k_h(\bar{t})$ given in Figure 8

Harmonic, n	Amplitude $\bar{e}(\bar{t})$ (μm)	Amplitude $k_h(\bar{t})$ (MN/m)
0	20·00	107·8
1	3·45	10·3
2	0·26	5·7
3	0·45	1·3
4	0·38	4·0
5	0·27	1·5
6	0·26	1·4

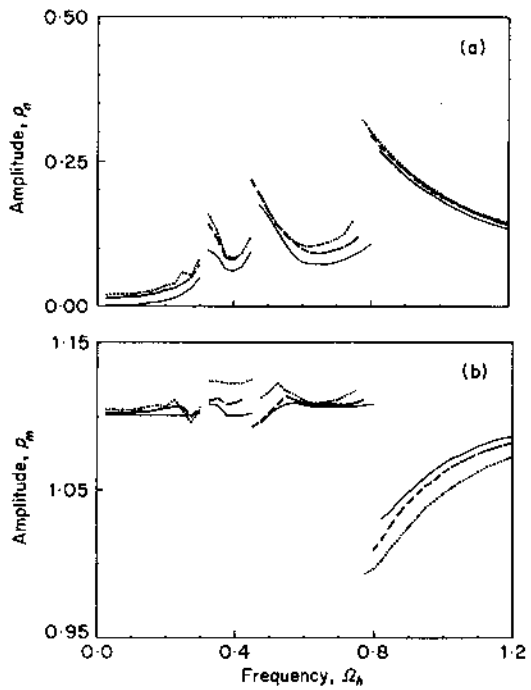

Figure 9. Frequency response spectra of a non-linear gear pair with periodic $\bar{e}(\bar{t})$ and $k_h(\bar{t})$; $F_m = 0{\cdot}1$, $F_{ah1} = 0{\cdot}05$, $F_{ah2} = 0{\cdot}02$, $F_{ah3} = 0{\cdot}01$, $\zeta_{33} = 0{\cdot}05$, $b_h = b_c$, $\varepsilon_1/\varepsilon_2 = 2$, $\varepsilon_1/\varepsilon_3 = 4$ and four different $\varepsilon_1 = \varepsilon$ values: (a) p_a versus Ω_h; (b) p_m versus Ω_h. Key as Figure 3 except - - - -, $\varepsilon = 0{\cdot}2$.

5.1. SINUSOIDAL $\bar{e}(\bar{t})$ AND $k_h(\bar{t})$

As in section 4, we assumed sinusoidal forms: $\kappa_{33}(t) = 1 + \varepsilon \cos(\Omega_h t + \phi_{h1})$ and $F_{ah}(t) = F_{ah1}\Omega_h^2 \cos(\Omega_h t + \phi_{e1})$. Equation (3a) reduces to an LTV matrix equation when gear backlash and radial bearing clearances are set to zero: i.e., $f_h(p(t)) = p(t)$ and $f_{bi}(y_{gi}(t)) = y_{gi}(t)$, $i = 1, 2$. In Figure 10 are shown $p_a(\Omega_h)$ and $y_{g1a}(\Omega_h)$ spectra of this LTV system under heavily loaded conditions with $F_m = 0{\cdot}1$, $F_{ah1} = 0{\cdot}01$, $\zeta_{33} = 0{\cdot}05$, $\zeta_{i3} = 0{\cdot}0125$ and $\zeta_{ii} = 0{\cdot}01$, $i = 1, 2$. Note that $y_{g1a} = y_{g2a}$ since the gear ratio is one [11]. As shown in Figure 10, the frequency response has peaks at $\Omega_h = \omega_I = 0{\cdot}4$ and $\Omega_h = \omega_{II} = 1{\cdot}25$, where ω_I and ω_{II} are the natural frequencies of the LTI system, corresponding to the first two coupled transverse-torsional modes [11]. In Figure 10(a), we observe a parametric resonance at $2\Omega_h = \omega_I$ similar to that for the gear pair model of section 4, whereas the parametric resonance at $2\Omega_h = \omega_{II}$ is more obvious in the $p_a(\Omega_h)$ spectrum of Figure 10(b) for a larger ε value. Again, like the LTV gear pair results of Figure 3, y_{g1a} and p_a are amplified with increasing ε in both resonance and off-resonance regions.

When the gear backlash $b_h = b_c$ has been introduced into this heavily loaded system the corresponding results are as given in Figure 11. The most significant effect of $k_h(\bar{t})$ is that it interacts with the gear backlash non-linearity to develop a jump discontinuity at the second primary resonance peak. This is clearly evident from the fact that either backlash or $k_h(\bar{t})$ alone cannot cause a jump for such a heavily loaded system. Besides an increase in amplitudes in Figures 11(a) and 11(b), chaotic and/or quasi-periodic solutions, which do not exist in heavily loaded time-invariant systems [11], are also predicted in the following regimes: $1{\cdot}35 < \Omega_h < 1{\cdot}65$ for $\varepsilon = 0{\cdot}2$ and $1{\cdot}25 < \Omega_h < 1{\cdot}7$ for $\varepsilon = 0{\cdot}4$. Similar to the LTV system response of Figure 10, parametric resonances at $2\Omega_h = \omega_I$ and $2\Omega_h = \omega_{II}$ are again observed here.

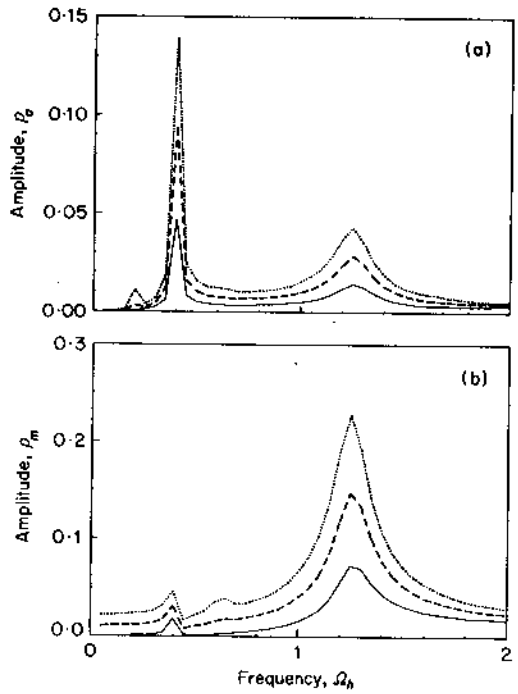

Figure 10. Frequency response spectra of the LTV geared rotor-bearing system of Figure 2(a) with sinusoidal $\bar{e}(\bar{t})$ and $k_h(\bar{t})$; $F_m = 0{\cdot}1$, $F_{ah1} = 0{\cdot}01$, $\zeta_{33} = 0{\cdot}05$, $\zeta_{i3} = 0{\cdot}0125$ and $\zeta_{ii} = 0{\cdot}01$, $\kappa_{ii} = 0{\cdot}5$, $b_h = b_{bi} = 0$, $i = 1, 2$ and four $\varepsilon_i = \varepsilon$ values: (a) y_{gia} versus Ω_h; (b) p_a vesus Ω_h. Key as Figure 9.

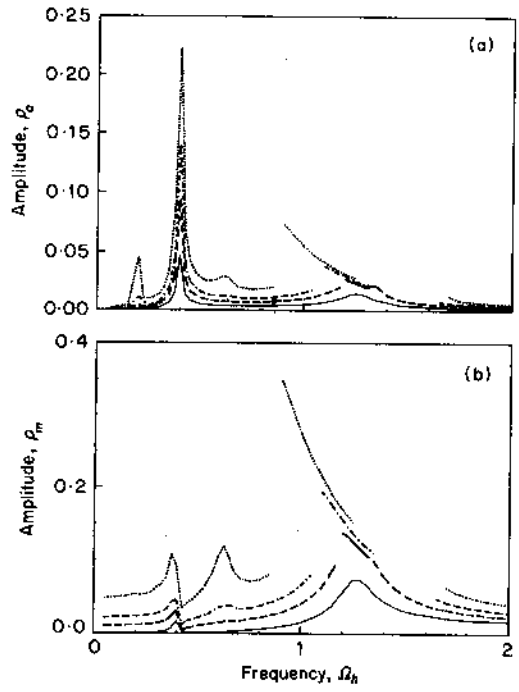

Figure 11. Frequency response spectra of a non-linear geared rotor–bearing system with sinusoidal $\bar{e}(\bar{t})$ and $k_h(\bar{t})$, $F_m = 0{\cdot}1$, $F_{ah1} = 0{\cdot}01$, $\zeta_{33} = 0{\cdot}05$, $\zeta_{i3} = 0{\cdot}0125$ and $\zeta_{ii} = 0{\cdot}01$, $\kappa_{ii} = 0{\cdot}5$, $b_h = b_c$, $b_{bi} = 0$, $i = 1, 2$, and four $\varepsilon_i = \varepsilon$ values: (a) y_{gia} versus Ω_h; (b) p_a versus Ω_h. Key as Figure 3.

Next, radial clearances in bearings $b_{bi} = b_c$ were considered for a heavily loaded system with zero gear backlash, $F_m = 1{\cdot}0$, $F_{ah1} = 0{\cdot}1$, $\zeta_{33} = 0{\cdot}05$, $\zeta_{i3} = 0{\cdot}0125$ and $\zeta_{ii} = 0{\cdot}01$, $i = 1, 2$. In this case, mesh stiffness variation and non-linearity exist in different components. As shown in Figure 12, ε again increases the amplitudes, but the spectrum shape is essentially the same. This is further evident from Figure 13, for a lightly loaded drive with $F_m = 1{\cdot}0$ and $F_{ah1} = 0{\cdot}5$. This suggests a weak interaction between the gear mesh stiffness variation and bearing non-linearities.

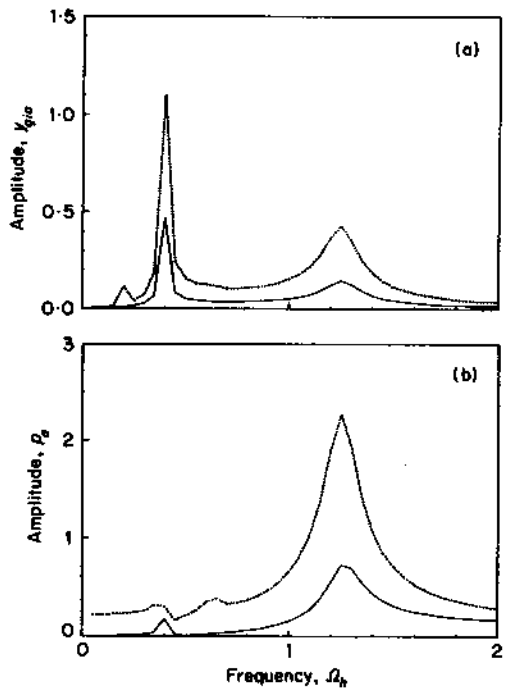

Figure 12. Frequency response spectra of a non-linear geared rotor-bearing system with sinusoidal $\bar{e}(\bar{t})$ and $k_h(\bar{t})$; $F_m = 1{\cdot}0$, $F_{ah1} = 0{\cdot}1$, $\zeta_{33} = 0{\cdot}05$, $\zeta_{i3} = 0{\cdot}0125$ and $\zeta_{ii} = 0{\cdot}01$, $\kappa_{ii} = 0{\cdot}5$, $b_{bi} = b_c$, $b_h = 0$, $i = 1, 2$, and two $\varepsilon_1 = \varepsilon$ values: (a) y_{gia} versus Ω_h, (b) p_a versus Ω_h. Key as Figure 9.

5.2. PERIODIC $\bar{e}(\bar{t})$ AND $k_h(\bar{t})$

In a manner similar to that for the gear pair analysis of section 4.4, we considered periodic $\kappa_{33}(t)$ and $F_{ah}(t)$ with three Fourier coefficients. In Figure 14 are shown spectra for $F_m = 0{\cdot}1$, $F_{ah1} = 0{\cdot}01$, $F_{ah}2 = 0{\cdot}004$, $F_{ah3} = 0{\cdot}002$, $\zeta_{33} = 0{\cdot}05$, $\zeta_{i3} = 0{\cdot}0125$ and $\zeta_{ii} = 0{\cdot}01$, $i = 1, 2$, $\varepsilon_1/\varepsilon_2 = 2$, $\varepsilon_1/\varepsilon_2 = 4$, and $\varepsilon_1 = \varepsilon = 0$, $0{\cdot}1$ and $0{\cdot}2$. Here only the gear backlash non-linearity ($b_h = b_c$ and $b_{bi} = 0$) was considered. Peaks at $\Omega_h = \omega_I/n$ and $\Omega_h = \omega_{II}/n$, $n = 1, 2, 3$ are predicted corresponding to excitation F_{ahr}. The periodic mesh stiffness enhances the alternating amplitudes over the values given by the time-invariant mesh stiffness case and introduces a jump discontinuity at the second primary resonance similar to the sinusoidal mesh stiffness case.

6. EXPERIMENTAL VALIDATION

6.1. SPUR GEAR PAIR DYNAMICS

First we compare our theory with experimental results of Kubo [34], as extracted from reference [19]. Kubo used a heavily damped ($\zeta_{33} = 0{\cdot}1$) four-square spur gear test rig,

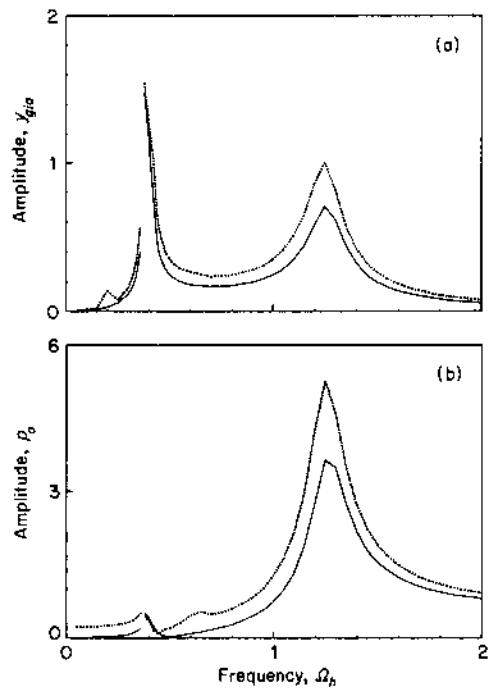

Figure 13. Frequency response spectra of a non-linear geared rotor–bearing system with sinusoidal $\bar{e}(\bar{t})$ and $k_h(\bar{t})$; $F_m = 1{\cdot}0$, $F_{ah1} = 0{\cdot}5$, $\zeta_{33} = 0{\cdot}05$, $\zeta_{i3} = 0{\cdot}0125$ and $\zeta_{ii} = 0{\cdot}01$, $\kappa_{ii} = 0{\cdot}5$, $b_{bi} = b_c$, $b_h = 0$, $i = 1, 2$, and two $\varepsilon_1 = \varepsilon$ values: (a) y_{gia} versus Ω_h; (b) p_a versus Ω_h. Key as Figure 9.

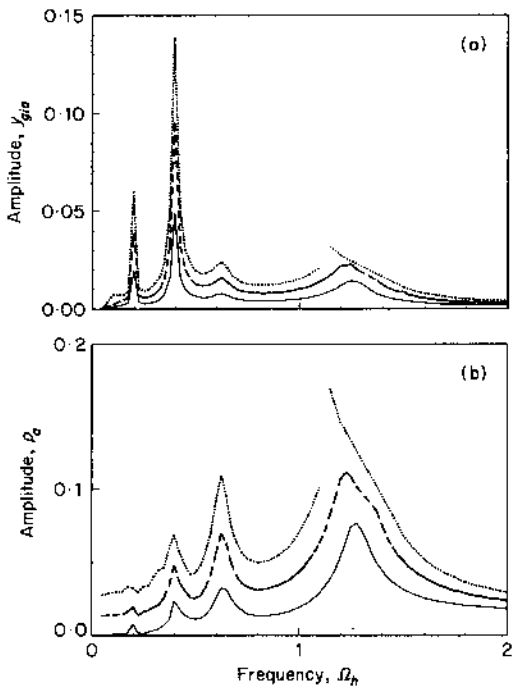

Figure 14. Frequency response spectra of a non-linear geared rotor–bearing system with periodic $\bar{e}(\bar{t})$ and $k_h(\bar{t})$; $F_m = 0{\cdot}1$, $F_{ah1} = 0{\cdot}01$, $F_{ah2} = 0{\cdot}004$, $F_{ah3} = 0{\cdot}002$, $\zeta_{33} = 0{\cdot}05$, $\zeta_{i3} = 0{\cdot}0125$ and $\zeta_{ii} = 0{\cdot}01$, $\kappa_{ii} = 0{\cdot}5$, $b_h = b_c$, $b_{bi} = 0$, $i = 1, 2$, $\varepsilon_1/\varepsilon_2 = 2$, $\varepsilon_1/\varepsilon_3 = 4$ and three $\varepsilon_1 = \varepsilon$ values: (a) y_{gia} versus Ω_h; (b) p_a versus Ω_h. Key as Figure 9.

and measured the dynamic factor as the ratio of the dynamic to static tooth root stresses. The experimental set-up was designed to support a gear pair with very stiff shafts and bearings. Therefore our gear pair model can represent the test rig adequately, similarly to our earlier study [10]. Parameters of the set-up [19, 34] are listed in Table 2. The static transmission error $\bar{e}(\bar{t})$ and time-varying mesh stiffness $k_h(\bar{t})$ of the gear pair tested has been predicted by using an existing elastic spur gear model [36] and then equation (4)

TABLE 2

Parameters for Kubo's test rig [34]

Number of teeth	25/25
I_{g1}, I_{g2} (kg m^2)	0·00115
m_{c1} (kg)	0·23
d_{g1}, d_{g2} (m)	0·094
k_b	Rigid
k_h (N/m)	3·8E8
$\bar{F}_m$ (N)	2295
$\tilde{e}$ (m)	1·9E−6
b_h (m)	0·1E−3
ζ_{33}	0·1
F_m	0·06
F_{ah}	0·0192
F_m/F_{ah}	3·12

was solved to predict the dynamic response. Here, we define the dynamic factor as the dynamic to static mesh force ratio which is equivalent to the dynamic factor calculation based on the stress analysis under the assumption that the change in the moment arm due to changes in the contact point is negligible. The envelope of measurements obtained by Kubo for several tooth pairs is compared in Figure 15 with our predictions. When the mesh stiffness $k_h(\bar{t})$ is assumed to be time-invariant, the predicted jump discontinuity is not as large as the jump seen in the experimental data, and the predicted transition frequency is higher than the measured value, as reported earlier in reference [10]. However, predictions improve significantly when sinusoidally varying $k_h(\bar{t})$ and $\bar{e}(\bar{t})$ at Ω_h are used, as given by equation (5). A sharp jump discontinuity is found which matches well

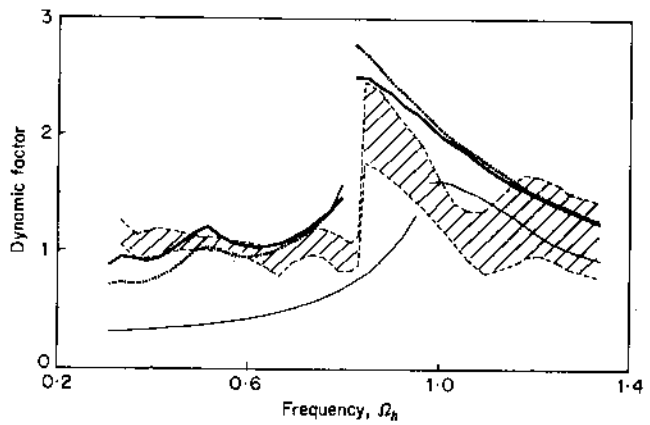

Figure 15. Comparison of theory with Kubo's experimental results [34]. – – –, Experiment; ——, $k_h \neq k_h(\bar{t})$, sinusoidal $\bar{e}(\bar{t})$; · · · ·, sinusoidal $k_h(\bar{t})$ and $\bar{e}(\bar{t})$; ——, periodic $k_h(\bar{t})$ and $\bar{e}(\bar{t})$.

with experiment, and the predicted dynamic factor is very close to the measured envelope. Finally, the prediction agrees with experiment even better when periodically varying $\bar{e}(\bar{t})$ and $k_h(\bar{t})$ with the first three Fourier coefficients are considered. This figure clearly shows that the time-invariant linear or non-linear model cannot predict the true dynamic behavior, as the time-varying mesh stiffness appears to yield a rather better model in the parameter range investigated.

6.2. GEARED ROTOR-BEARING SYSTEM

As the second example case, experimental results of Munro [2] are compared with our geared rotor–bearing model of Figure 2(a) and equation (3). These experimental results were used earlier to validate our previous time-invariant multi-degree-of-freedom non-linear system [11] in which we had to reduce the damping ratio and increase the excitation $\bar{e}(\bar{t})$ in order to correlate theory with experiment. Now we go back to the original system parameters given in references [2, 11], and predict the dynamic transmission error spectra using both time-varying and time-invariant gear mesh stiffness formulations for a three-degree-of-freedom non-linear model with gear backlash and linear bearings; see Table 3 for the parameters of the experimental set-up [2] . Results at the design load which correspond to the minimum excitation $\bar{e}(\bar{t})$ are compared in Figure 16. In this case, the mean load to alternating load ratio $\hat{F} = F_m/F_{ah1}$ is very large, say $\hat{F} \approx 30$. The time-invariant stiffness model prediction differs considerably from the experimental results in Figure 16. Predicted amplitudes are considerably lower than the measurements, and a significant jump discontinuity found experimentally around the second natural frequency ω_{II} is not even predicted by this formulation. But when the periodically varying mesh stiffness is considered, our model predicts the frequency response accurately, including the jump discontinuity. The reason for a large jump around ω_{II} for a very heavily loaded system ($\hat{F} \approx 30$) is now clear. The second natural frequency ω_{II} of the corresponding LTI system is nearly twice the first natural frequency ω_I. This forces the second primary

TABLE 3

Parameters for Munro's test rig [2]

Number of teeth	32/32
I_{g1}, I_{g2} (kg m^2)	0·136
m_{g1}, m_{g2} (kg)	31·1
d_{g1}, d_{g2} (m)	0·2
b_h (m)	0·12E−3

	Design load (*DL*)	3/4 *DL*	1/2 *DL*	1/4 *DL*
$\bar{F}_m$ (N)	3782	2836	1891	947
k_h (N/m)	3·44E8	3·22E8	3·01E8	2·72E8
$\bar{e}$ (m)	3·5E−7	1·06E−6	1·78E−6	2·36E−6
F_m	0·183	0·146	0·105	0·058
F_{ah}	0·0058	0·0178	0·0296	0·0393
κ_{11}, κ_{22}	0·950	0·966	0·983	1·007
κ_{13}, κ_{23}	0·242	0·242	0·242	0·242
ζ_{11}, ζ_{22}	0·01	0·01	0·01	0·01
ζ_{13}, ζ_{23}	0·00375	0·00375	0·00375	0·00375
ζ_{33}	0·015	0·015	0·015	0·015

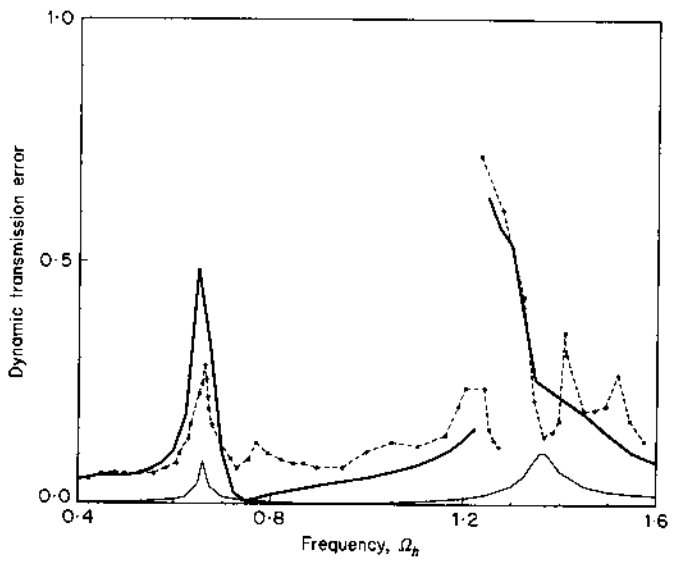

Figure 16. Comparison of theory with Munro's experiment at the design load [2]. – – – – –, Experiment; ——, time-varying mesh stiffness; ——, time-invariant mesh stiffness.

resonance at $\Omega_h \approx \omega_{II}$ to coincide with the parametric resonance at $\Omega_h \approx 2\omega_I$; consequently, a very large jump discontinuity is developed.

At 3/4 of the design load with $\hat{F} \approx 10$, the effect of $k_h(\bar{t})$ is observed in Figure 17. Although the time-invariant model predicts the jump at ω_{II}, predicted amplitudes are far below the measurements. The inclusion of $k_h(\bar{t})$ improves predictions drastically. Similarly at 1/2 and 1/4 design loads, mesh stiffness variation, as shown in Figures 18 and 19, respectively, affects the frequency response significantly and yields predictions closer to the measurements.

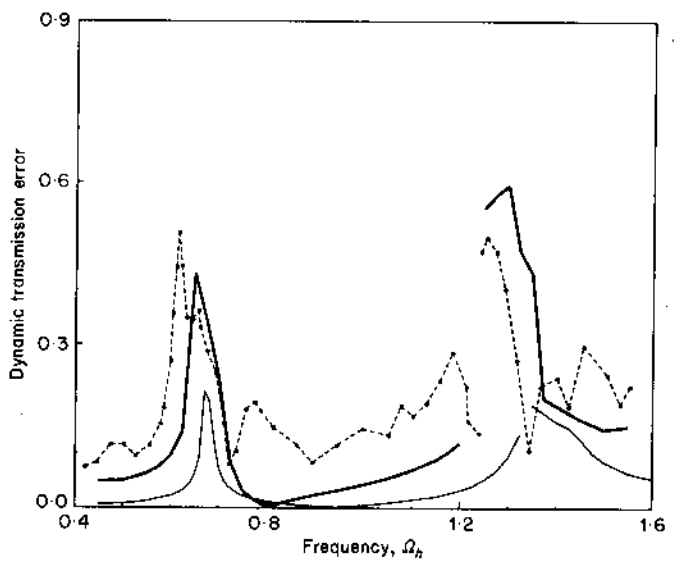

Figure 17. Comparison of theory with Munro's experiment at 3/4 of the design load [2]. Key as Figure 16.

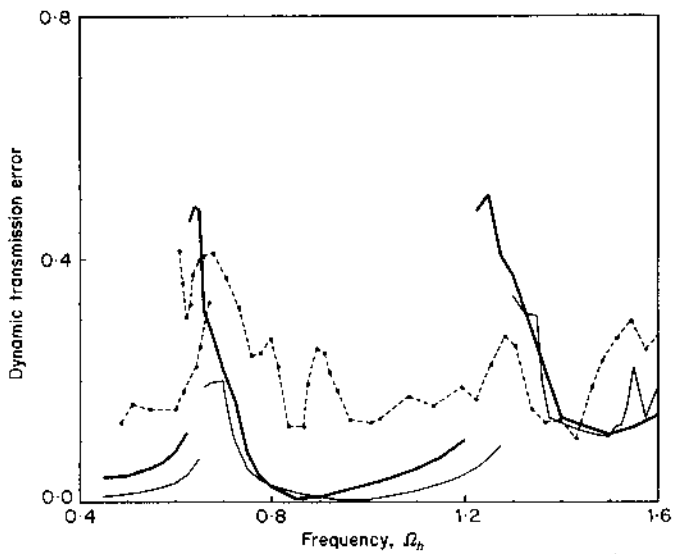

Figure 18. Comparison of theory with Munro's experiment at 1/2 of the design load [2]. Key as Figure 16.

7. CONCLUDING REMARKS

This study of the non-linear dynamics of a geared rotor-bearing system with time-varying mesh stiffness $k_h(\bar{t})$, as excited by the static transmission error under a mean load, has resolved a number of fundamental issues. First, the interaction between time-varying mesh stiffness $k_h(\bar{t})$ and mean torque load has been understood. Second, frequency response of the corresponding LTV system has been studied, and the resonances associated with parametric and forced excitations have been identified. Finally, dynamic interactions between $k_h(\bar{t})$ and system non-linearities associated with gear backlash and radial clearances in rolling element bearings have been investigated; a strong interaction between

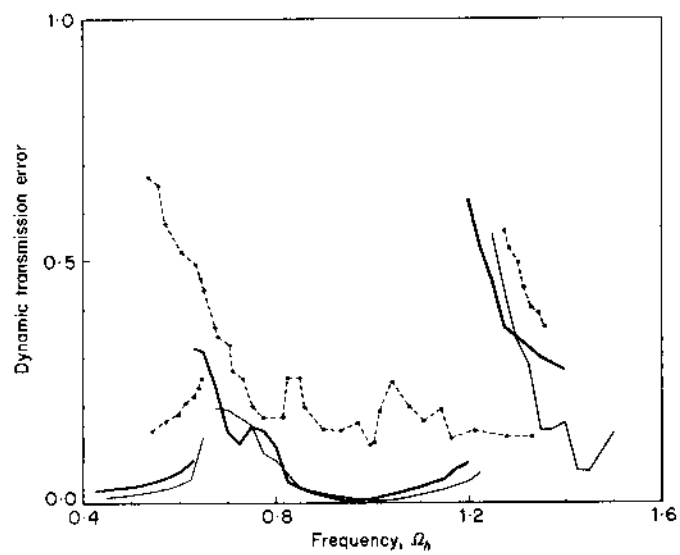

Figure 19. Comparison of theory with Munro's experiment at 1/4 of the design load [2]. Key as Figure 16.

$k_h(\bar{t})$ and gear backlash is found, whereas the coupling between $k_h(\bar{t})$ and bearing non-linearities is weak.

ACKNOWLEDGMENTS

We thank NASA Lewis Research Center for supporting this study and D. R. Houser for his guidance.

REFERENCES

1. H. N. OZGUVEN and D. R. HOUSER 1988 *Journal of Sound and Vibration* **121**, 383–411. Mathematical models used in gear dynamics—a review.
2. R. G. MUNRO 1962 *Ph.D. Dissertation, Cambridge University.* The dynamic behaviour of spur gears.
3. M. HORTEL 1967 *Proceedings of the Fourth Conference on Non-linear Oscillations*, 337–346. Forced damped vibrations in a nonlinear parametric system of gears with several degrees of freedom.
4. K. UMEZAWA, T. SATA and J. ISHIKAWA 1984 *Bulletin of the Japan Society of Mechanical Engineers* **38**, 102–109. *Simulation of rotational vibration of spur gears.*
5. H. H. LIN, R. L. HUSTON and J. J. COY 1988 *Journal of Mechanisms, Transmission, and Automation in Design, Transactions of the American Society of Mechanical Engineers* **110**, 221–225. On dynamic loads in parallel shaft transmissions, Part I—modelling and analysis.
6. H. H. LIN, R. L. HUSTON and J. J. COY 1988 *Journal of Mechanisms, Transmissions, and Automation in Design, Transactions of the American Society of Mechanical Engineers* **110**, 226–229. On dynamic loads in parallel shaft transmissions, Part II—parameter study.
7. M. BENTON and A. SEIREG 1978 *Journal of Mechanical Design, Transactions of the American Society of Mechanical Engineers* **100**, 26–32. Simulation of resonances and instability conditions in pinion-gear systems.
8. M. BENTON and A. SEIREG 1981 *Journal of Mechanical Design, Transactions of the American Society of Mechanical Engineers* **103**, 372–378. Factors influencing instability and resonances in geared systems.
9. K. L. WANG and H. S. CHENG 1981 *Journal of Mechanical Design, Transactions of the American Society of Mechanical Engineers* **103**, 177–187. A numerical solution to the dynamic load, film thickness, and surface temperatures in spur gears, Part I—analysis.
10. A. KAHRAMAN and R. SINGH 1990 *Journal of Sound and Vibration* **142**, 49–75. Non-linear dynamics of a spur gear pair.
11. A. KAHRAMAN and R. SINGH 1991 *Journal of Sound and Vibration* **144**, 469–506. Non-linear dynamics of a geared rotor-bearing system with multiple clearances.
12. R. J. COMPARIN and R. SINGH 1989 *Journal of Sound and Vibration* **134**, 259–290. Nonlinear frequency response characteristics of an impact pair.
13. R. SINGH, H. XIE and R. J. COMPARIN 1989 *Journal of Sound and Vibration* **131**, 177–196. Analysis of an automotive neutral gear rattle.
14. C. C. WANG 1978 *Journal of Mechanical Design, Transactions of the American Society of Mechanical Engineers* **100**, 363–373. Rotational vibration with backlash: Part 1.
15. C. C. WANG 1981 *Journal of Mechanical Design, Transactions of the American Society of Mechanical Engineers* **103**, 387–397. Rotational vibration with backlash: Part. 2.
16. K. ICHIMARU and F. HIRANO 1974 *Journal of Engineering for Industry, Transactions of the American Society of Mechanical Engineers* **96**, 373–381. Dynamic behavior of heavily-loaded spur gears.
17. T. SAKAI, Y. DOI, K. YAMATOMO, T. OGASAWARA and M. NARITA 1981 *SAE Paper* 810773. Theoretical and experimental analysis of rattling noise of automotive gearbox.
18. S. OHNUMA, Y. SHIGETARO, I. MINEICHI and T. FUJIMOTO 1985 *SAE Paper* 850979. Research on the idling rattle of manual transmission.
19. H. N. OZGUVEN and D. R. HOUSER 1988 *Journal of Sound and Vibration* **125**, 71–83. Dynamic analysis of high speed gears by using loaded static transmission error.
20. F. KUCUKAY 1984 *Proceedings of the Third Conference on Vibrations of Rotating Machinery, Institution of Mechanical Engineers* 73–79. Dynamic loads in gear teeth.

21. R. C. AZAR and F. R. E. CROSSLEY 1977 *Journal of Engineering for Industry, Transactions of the American Society of Mechanical Engineers* **99**, 792–798. Digital simulation of impact phenomenon in spur gear systems.
22. K. NAKAMURA 1967 *Bulletin of Japanese Society of Mechanical Engineers* **10**, 846–854. Tooth separation and abnormal noise on power transmission gears.
23. H. WINTER and M. KOJIMA 1981 *Proceedings of the International Symposium on Gearing and Power Transmissions, Tokyo*, C-12. A study on the dynamics of geared system—estimation of overload on gears in system.
24. R. KASUBA and J. W. EWANS 1981 *Journal of Mechanical Design, Transactions of the American Society of Mechanical Engineers* **103**, 398–409. An extended model for determining dynamic loads in spur gearing.
25. R. W. CORNELL and W. W. WESTERVELT 1978 *Journal of Mechanical Design, Transactions of the American Society of Mechanical Engineers* **100**, 69–76. Dynamic tooth loads and stressing for high contact ratio spur gears.
26. H. N. OZGUVEN 1989 *Research Report, The Ohio State University, Columbus, Ohio.* Further work on DYTEM computer code.
27. A. H. NAYFEH and D. T. MOOK 1979 *Nonlinear Oscillations.* New York: Wiley-Interscience.
28. A. H. NAYFEH 1985 *Problems in Perturbation.* New York: Wiley-Interscience.
29. J. A. RICHARDS 1983 *Analysis of Periodically Time-Varying Systems.* New York: Springer-Verlag.
30. H. TROGER and C. S. HSU 1977 *Journal of Applied Mechanics, Transactions of the American Society of Mechanical Engineers* **44**, 179–181. Response of a nonlinear system under combined parametric and forcing excitation.
31. C. S. HSU and W. H. CHENG 1974 *Journal of Applied Mechanics, Transactions of the American Society of Mechanical Engineers* **41**, 371–378. Steady state response of a dynamical system under combined parametric and forcing excitation.
32. N. HAQUANG, D. T. MOOK and R. H. PLAUT 1987 *Journal of Sound and Vibration* **118**, 425–439. A non-linear analysis of the interactions between parametric and external excitations.
33. N. HAQUANG 1986 *Ph.D. Thesis, Virginia Polytechnic Institute and State University.* Response of non-linear structural systems to multifrequency excitations.
34. A. KUBO, K. YAMADA, T. AIDA and S. SATO 1972 *Transactions of Japan Society of Mechanical Engineers* **38**, 2692–2715. Research on ultra high speed gear devices (reports 1–3).
35. IMSL INC. 1987 *User's Manual.*
36. M. S. TAVAKOLI and D. R. HOUSER 1986 *Journal of Mechanisms, Transmissions and Automation in Design, Transactions of the American Society of Mechanical Engineers* **108**, 86–95. Optimum profile modifications for the minimization of static transmission errors of spur gears.

APPENDIX: LIST OF SYMBOLS

A	amplitude of the solution associated with the first time scale
b	backlash
c, C	damping
cc	complex conjugate
d	diameter
D	partial derivative with respect to time scale
e	static transmission error
f	non-linear displacement function
F	force
I	rotary inertia
k, K	stiffness
m, M	mass
p	relative displacement
q	displacement
t	time
T	torque or time scale
y	transverse displacement
ε	k_{ha}/k_{hm} ratio
ϕ	phase angle
κ	dimensionless stiffness
Λ	a quantity

θ rotational displacement
ω natural frequency
Ω excitation frequency
ζ damping ratio

Subscripts

a alternating component
b bearing
c, $c1$ reference quantities
e static transmission error
$g1$ pinion
$g2$ gear
h gear mesh
m mean component
n natural
r an index
T torque
I, II modal index

Superscripts

$\tilde{}$ dimensional quantities† or complex conjugate
$\bar{}$ amplitude of a harmonic function
$\dot{}$ derivative with respect to time
$\hat{}$ force ratio

† All dimensionless quantities are without any superscript.